Induction of Synthetic Lethality by Activation of Mitochondrial ClpP and Inhibition of HDAC1/2 in Glioblastoma

Trang T.T. Nguyen[1], Enyuan Shang[2], Salveena Schiffgens[1], Consuelo Torrini[1], Chang Shu[1], Hasan Orhan Akman[3], Varun V. Prabhu[4], Joshua E. Allen[4], Mike-Andrew Westhoff[5], Georg Karpel-Massler[6], and Markus D. Siegelin[1]

ABSTRACT

Purpose: Novel therapeutic targets are critical to unravel for the most common primary brain tumor in adults, glioblastoma (GBM). We have identified a novel synthetic lethal interaction between ClpP activation and HDAC1/2 inhibition that converges on GBM energy metabolism.

Experimental Design: Transcriptome, metabolite, and U-13C-glucose tracing analyses were utilized in patient-derived xenograft (PDX) models of GBM. Orthotopic GBM models were used for *in vivo* studies.

Results: We showed that activation of the mitochondrial ClpP protease by mutant ClpP (Y118A) or through utilization of second-generation imipridone compounds (ONC206 and ONC212) in combination with genetic interference of HDAC1 and HDAC2 as well as with global (panobinostat) or selective (romidepsin) HDAC inhibitors caused synergistic reduction of viability in GBM model systems, which was mediated by interference with tricarboxylic acid cycle activity and GBM cell respiration. This effect was partially mediated by activation of apoptosis along with activation of caspases regulated chiefly by Bcl-xL and Mcl-1. Knockdown of the ClpP protease or ectopic expression of a ClpP D190A mutant substantially rescued from the inhibition of oxidative energy metabolism as well as from the reduction of cellular viability by ClpP activators and the combination treatment, respectively. Finally, utilizing GBM PDX models, we demonstrated that the combination treatment of HDAC inhibitors and imipridones prolonged host survival more potently than single treatments or vehicle *in vivo*.

Conclusions: Collectively, these observations suggest that the efficacy of HDAC inhibitors might be significantly enhanced through ClpP activators in model systems of human GBM.

Introduction

There is a significant demand for durable treatments for the most common primary brain tumor in adults, glioblastoma (GBM; refs. 1–4). Contrasting the advances in glioma biology, still the prognosis is unfavorable. Single-cell sequencing technologies have recently confirmed earlier findings about the heterogeneity of these tumors (2–4). From these observations there is little doubt that simultaneous targeting of multiple pathways is necessary to accomplish durable responses (5–12).

The discovery of imipridones has impacted the neuro-oncology field since several clinical trials have been launched with these compounds (13–15). The most studied member out of this family is ONC201 that has been used for most clinical trials both in central nervous system and other peripheral malignancies (solid and non-solid cancers; ref. 15). While ONC201 appeared to have a more limited efficacy, the chemical derivatives, ONC206 and ONC212, display higher potency against tumor cells, including GBM (15, 16). ONC206 has entered a phase I trial for solid central nervous system malignancies, including glioblastoma and gliosarcoma (NCT04541082). Although initially discovered as substances that induce the cytokine, TRAIL, more recently the actual binding target has been identified by two groups, which turned out to be the mitochondrial ClpP protease (17–19). In this context, systematic elucidation of the mitochondrial ClpP protease as a therapeutic target has not been performed and the identification of novel synthetic lethal interactions, involving the activation of these enzymes, might result in the development of novel therapeutic venues. Upon its activation, the ClpP protein cleaves the respiratory complexes and thereby diminishes cellular respiration and ATP production through the process of oxidative phosphorylation (17–19). In this context, it has been shown that the ClpP Y118A mutant is constitutively active, whereas the ClpP (D190A) renders the enzyme inactive (17–19). Energy metabolism beyond the classical Warburg effect has received significant attention in oncology since recent research clearly outlines that oxidative metabolism is a necessity for tumors to grow (20–23). To this end, interference with oxidative metabolism may be a valid approach for a strong consideration as a potential novel treatment modality for recalcitrant malignancies (such as GBM). However, efficient approaches to accomplish this are still lacking.

Although HDAC inhibitors have fallen short of expectations in several preceding clinical trials, these reagents remain interesting for a couple of reasons (24). First, HDAC inhibitors, such as romidepsin and

[1]Department of Pathology and Cell Biology, Columbia University Medical Center, New York, New York. [2]Department of Biological Sciences, Bronx Community College, City University of New York, Bronx, New York. [3]Department of Neurology, Columbia University Medical Center, New York, New York. [4]Chimerix, Inc., Durham, North Carolina. [5]Department of Pediatrics and Adolescent Medicine, Ulm University Medical Center, Ulm, Germany. [6]Department of Neurosurgery, Ulm University Medical Center, Ulm, Germany.

Note: Supplementary data for this article are available at Clinical Cancer Research Online (http://clincancerres.aacrjournals.org/).

Corresponding Author: Markus D. Siegelin, Columbia University Medical Center, 630 W. 168th Street, P&S 14-511, New York, NY 10032. Phone: 212-305-1993; E-mail: ms4169@cumc.columbia.edu

Clin Cancer Res 2022;28:1881–95

doi: 10.1158/1078-0432.CCR-21-2857

Translational Relevance

Glioblastoma, the most common primary brain tumor in adults, requires better treatments in light of the fact that the standard of care provides only a small clinical benefit in patients. Histone-deacetylase inhibitors (HDACi), for example, panobinostat, and imipridones (e.g., ONC201), have entered clinical trials and are known to penetrate the blood–brain barrier, which is a critical prerequisite for glioblastoma therapy. In addition, both compounds have displayed antiglioma activity and ONC201 is known to enhance the efficacy of the standard of care (i.e., radiation) in preclinical model systems of glioblastoma. The current findings suggest that a combination therapy of second-generation imipridones and HDACi exerts significant antiglioma activity in relevant disease model systems of glioblastoma. Therefore, additional clinical consideration should be given to this potentially promising therapeutic regimen either in the presence or absence of the standard of care.

panobinostat, are FDA approved, albeit for other indications than GBM. Second, in the context of GBM, they might not have been studied on the right patient populations. Third, panobinostat is known to penetrate the blood–brain barrier (25). Fourth, drug combinations, involving HDAC inhibitors, might still be efficacious in patients and may not have received enough attention in the past. Thus, these compounds still bear promise. The concept that the therapeutic combination of activation of the ClpP protease (through imipridones) along with HDAC1/2 inhibition may lead to enhanced reduction of GBM cell viability was based on our previous finding that HDAC inhibitors enhance pro-survival GBM cell respiration and fatty acid oxidation (12). In contrast, imipridones (ONC201, ONC206, ON212) suppress respiration in part through down-regulation of the respiratory complexes (16). Therefore, combining the two modalities might have synergistic killing effects in GBM cells.

In the present work, we discovered that genetic (ClpP Y118A) and pharmacological activation of the ClpP protease combined with genetic or pharmacologic inhibition of HDAC1/2 induced synergistic reduction of cellular viability in human GBM model systems *in vitro* and *in vivo*, which is mediated upstream through disruption of oxidative energy metabolism and executed downstream by regulation of Bcl-2 family proteins.

Materials and Methods

Cell cultures

All cell lines were incubated at 37°C in an atmosphere containing 5% CO_2. GBM12 and GBM14 (mesenchymal subtypte), GBM61 (proneural subtype), and GBM43 (classical subtype) cells were obtained from Dr. Jann Sarkaria (Mayo Clinic, Rochester, MN). U251 cells were obtained from Sigma. GL261 cells was obtained from Repository of Tumors and Tumor Cell Lines, NCI (Bethesda, MD). From ATCC, 293T (ATCC CRL-3216) was obtained. Cells were cultured in DMEM (Fisher Scientific, MT10013CV), 10% FBS (Gemini), and 100 μg/mL of primocin (Invivogen, ant-pm-1). For the treatment experiment, cells were cultured in DMEM containing 1.5% FBS. All the cells were performed with passages four to nine. Astrocyte was purchased from ScienceCell Research Laboratories and were cultured in the media in DMEM, 10% FBS, N-2 Supplement (Thermo Fisher, 17502048), and 100 μg/mL of primocin. NCH644 stem-like glioma cells (Cell Line Services, 820403) were cultured in StemPro NSC SFM (Thermo Fisher, A1050901) with 100 μg/mL primocin for maintenance and for drug treatment. The cell line repositories performed the authentications and *Mycoplasma* contamination was excluded by the original source.

Reagents

Imipridones (ONC201, ONC206, and ONC212) were obtained from Chimerix Inc./Oncoceutics. Panobinostat (HY-10224) and romidepsin (HY-15149) were purchased from MedchemExpress. Z-VAD-FMK (S7023) and ATP disodium (S1985) were purchased from Selleckchem. Puromycin dihydrochloride (P9620) was purchased from Sigma. A 10 mmol/L working solution in dimethylsulfoxide (DMSO) was prepared for all reagents with a final concentration below 0.1% (v/v).

Cell viability assays

A 96-well plate was seeded with 3,000 cells overnight and was treated with target drugs for 72 hours prior to analyzing cellular proliferation by CellTiter-Glo assays (Promega, G7571). Bliss analysis was performed to detect synergistic, additive, or antagonistic effects of combination drug treatment by using the formula: $\frac{Fa+Fb-FaFb}{Fc}$. *Fa* is the fractional response to drug A; *Fb* is the fractional response to drug B; and *Fc* is the fractional response to the combination treatment with drug A and B. If the ratio was < 0.9, the effect was described as antagonistic. If the ratio was from 0.9 to 1.1, the effect was described as addictive. If the ratio was > 1.1, the effect was described as synergistic. In the ATP rescue experiments, cell viability was performed by CyQUANT Cell Proliferation Assay (Thermo Fisher, C7026).

Flow cytometry

Cells were seeded in a 12-well plate with density 30,000 cells per well overnight. FITC Annexin V/propidium iodide (BD Biosciences, 556420) was used to detect the apoptosis and necrosis cells. Signal was detected on a LSRII flow cytometry (BD) and the data was analyzed with FlowJo software (version 8.7.1; Tree Star).

Microarray and subsequent gene-set enrichment analysis

The experiment is comprised of 8 Human Gene 2.0 ST arrays, profiling GBM14 cells (PDX glioblastoma cell line) treated with DMSO vehicle control, the DRD2 antagonist/ClpP agonist ONC206, the histone deacetylase (HDAC) inhibitor romidepsin, or the combination of the two ($n = 2$ per experimental group). The arrays were normalized at the same time by employing the Robust Multiarray Average (RMA) algorithm with a chip definition file that involves unique Entrez Gene identifiers (Brainarray version 24.0.0). GSEA pathway analysis was performed with MSigDB version 7.1. The experiments used in this study were deposited at GEO: GSE166111.

Western blot and protein capillary electrophoresis

Cells were lysed in the Laemmli buffer (Bio-Rad) containing 1X protease and phosphatase inhibitor cocktail (Thermo Fisher, 78440). For standard Western blot, samples were run on a 4%–12% SDS PAGE gel (Invitrogen, NP0321BOX) and were transferred to a polyvinylidene difluoride membrane. The western blots were captured by using the Azure (C300) imaging system (Azure Biosystems). Protein capillary electrophoresis was detected by using the Wes instrument (Protein-Simple). The antibodies were used in the standard Western blot: acetyl-histone H3 (Lys27; D5E4; CST 8173, 1:500), histone H3 (CST 14269; 1:500), PARP (CST 9532; 1:500), cCP9 (CST 7237; 1:500), cCP3 (CST 9665; 1:500), β-actin (Sigma Aldrich A1978, clone AC15; 1:2,000),

Mcl-1 (CST 5453; 1:500), Bcl-xL (CST 2764; 1:500), SDHA (Abcam, ab123545; 1:500), OXPHOS (Abcam, ab110411;1:500), ClpP (B-12; Santa Cruz Biotechnology Inc, sc-271284; 1:500), ClpX (Abcam, ab203694, 1:500), Goat anti-Rabbit IgG (H+L) Secondary Antibody, HRP (Thermo Fisher, 31460), and Goat anti-Mouse IgG (H+L) Secondary Antibody, HRP (Thermo Fisher, 31430). The antibodies were used in the protein capillary electrophoresis: HDAC1 (CST 34589; 1:25), HDAC2 (CST 57156; 1:25), and Vinculin (Abcam ab129002, 1:500).

Real-time PCR analysis

Total RNA was extracted by using miRNAeasy Mini Kit from QIAGEN (217004). cDNA was synthesized by using the cDNA supermix kit (101414–106) and was amplified by using power SYBR green RT-PCR reagents kit from Quantabio (101414–276) with the condition 95°C for 10 minutes, followed by 40 cycles of 95°C for 15 seconds, 60°C for 30 seconds, and 72°C for 30 seconds, on a qPCR Instrument (Quantabio). All RT-PCR was performed in quadruplicate and the average fold changes were calculated based on 18S in the threshold cycle (Cq). Primer sequences are in the Table 1 (Supplementary Table S1).

siRNA transfection and lentivirus transduction

siRNAs were purchased from Dharmacon: non-targeting siRNA-pool (scramble; D-001810–10–20), CLPP siRNA-pool (L-005811–00–0005), HDAC1 siRNA (L-003493–00–0005), HDAC2 siRNA (L-003495–02–0005), Mcl1 siRNA (J-004501–17–0005). Bcl-xL (CST, 6362) siRNA was obtained from Cell Signaling Technology. Transfections were performed with Lipofectamine RNAiMAX (Invitrogen, 13778075) according to manufacturers' instructions. CLPP shRNA (TRCN0000046858, TRCN0000046859, and TRCN0000046860), HDAC1 shRNA (TRCN0000195103 and TRCN0000195467), and HDAC2 shRNA (TRCN0000004819 and TRCN0000195198) were purchased from Sigma. Mouse CLPP adenovirus (ADV-255686) was purchased from Vector Biolabs. pLX307 Luciferase (117734) was purchased from Addgene. The lentiviral constructs (empty vector, CLPP- wild type and CLPP-D190A) in pCDH-EF1a-MCS-BGH-PGK-GFP-T2A-Puro (Systems Biosciences) were a gift from Drs. Schimmer (University of Toronto, Toronto, Canada) and Andreeff (Department of Leukemia, MD Anderson Cancer Center, Houston, Texas). Lentivirus production was performed by transfection of pMD2.G, psPAX2, and the relevant lentivirus transfer plasmid into 293T cells. The viral supernatant was collected over 72 hours. The viral particles were filtered and concentrated before they were used for transduction of target GBM cells.

Isotope tracing

GBM14 cells were seeded with a density of 1×10^6 cells per 10-cm dish and were exposed to DMEM no glucose, no glutamine, and no phenol red (Thermo Fisher, A1443001), containing 25 mmol/L (U-^{13}C6) D-Glucose (Cambridge Isotope Laboratories, Inc, CLM-1396–2), 4 mmol/L Glutamine (Fisher Scientific, 15410314), and 1.5% dialyzed FBS (Thermo Fisher, A3382001) for 24 hours. Polar metabolites were analyzed by Metabolomics Core Facility at Weil Cornell (New York, NY).

Chromatin immunoprecipitation RT-PCR

Cells were seeded with density 4×10^6 cells per 15-mm dish and were extracted according to the company instructions kit (SimpleChIP Enzymatic Chromatin IP Kit, CST 9003). Chromatin immunoprecipitation (chIP) samples were incubated with H3K27ac antibody (CST 4535, 10 μL/sample) or rabbit IgG antibody (CST 2729, 1 μL/sample). Primer sequences are listed in Table 1 (Supplementary Table S1).

Extracellular flux analysis

A XFe24 cell culture microplate (Agilent) was seeded at 3×10^4 cells per well DMEM medium containing 5 mmol/L glucose, 1 mmol/L pyruvate, and 10% FBS and allowed to attach overnight. Cells were treated with target drugs in the medium containing 5 mmol/L glucose, 1 mmol/L pyruvate, and 1.5% FBS for 24 hours. The oxygen consumption rate (OCR) was measured with a Seahorse XFe24 Analyzer (Agilent) using the mito stress assay kit (Agilent, 103015–100) in the Seahorse XF base medium (Agilent, 102353–100) containing 10 mmol/L glucose, 2 mmol/L glutamine, and 1 mmol/L pyruvate.

Subcutaneous xenograft, orthotopic glioblastoma PDX, and syngeneic model

A total of 3×10^6 GBM12 and GBM43 cells were implanted subcutaneously into the flanks of 6- to 8-week-old SCID/SHO mice (NCRNU-F sp/sp, CrTac:NCr-Foxn1nu). Drugs were dissolved in a mixture containing DMSO, cremophor EL (Sigma, 61791–12–6), Ethyl Alcohol (Pharmco-Aaper, 200 Proof), and PBS at the ratio: 10:32:8:50 (v/v/v/v). Tumor sizes were measured with a caliper and were calculated as (length × width^2)/2 three times a week. GBM12 and GL261 cells were intracranially injected at 3 mm lateral of the bregma and 3 mm down in 6- to 8-week-old SCID/SHO mice or B6-F (C57BL/6NTac), respectively. Treatments were given until the animals became moribund or when neurologic deficits were observed (retardation, lethargy, seizures). The survival curve was analyzed by Kaplan–Meier survival fractions and log-rank test was employed for the statistical significance.

Statistical analysis

Statistical significance was assessed by two-tailed Student t test or ANOVA (for multiple comparisons) using Prism version 9 (GraphPad). A $P \le 0.05$ was considered statistically significant.

Data availability statement

The data generated in this study are publicly available in Gene Expression Omnibus (GEO) at GSE166111.

Study approval

All procedures were conducted in accordance with Animal Welfare Regulations and were approved by the Institutional Animal Care and Use Committee (IACUC) at the Columbia University Medical Center (AC-AABC6505 and AC-AAAV7451).

Results

Activation of the ClpP protease along with inhibition of HDAC1/2 causes synthetic lethality in GBM model systems

To identify novel synthetic lethal interactions, involving ClpP protease activators, we focused on their principal feature to reduce oxidative energy metabolism. We hypothesized that pathways that upon their inhibition, for example, HDAC1/2 inhibition, facilitate an oxidative energetic phenotype (12) were likely to synergize with ClpP protease activators (**Fig. 1A–D**). Therefore, we utilized the selective HDAC1/2 inhibitor romidepsin and the ClpP protease activator, ONC206, and assessed how these compounds would alter the transcriptome of the short-terzm GBM14 PDX cell culture following single and combination treatment. To this end, GBM14 cells were treated

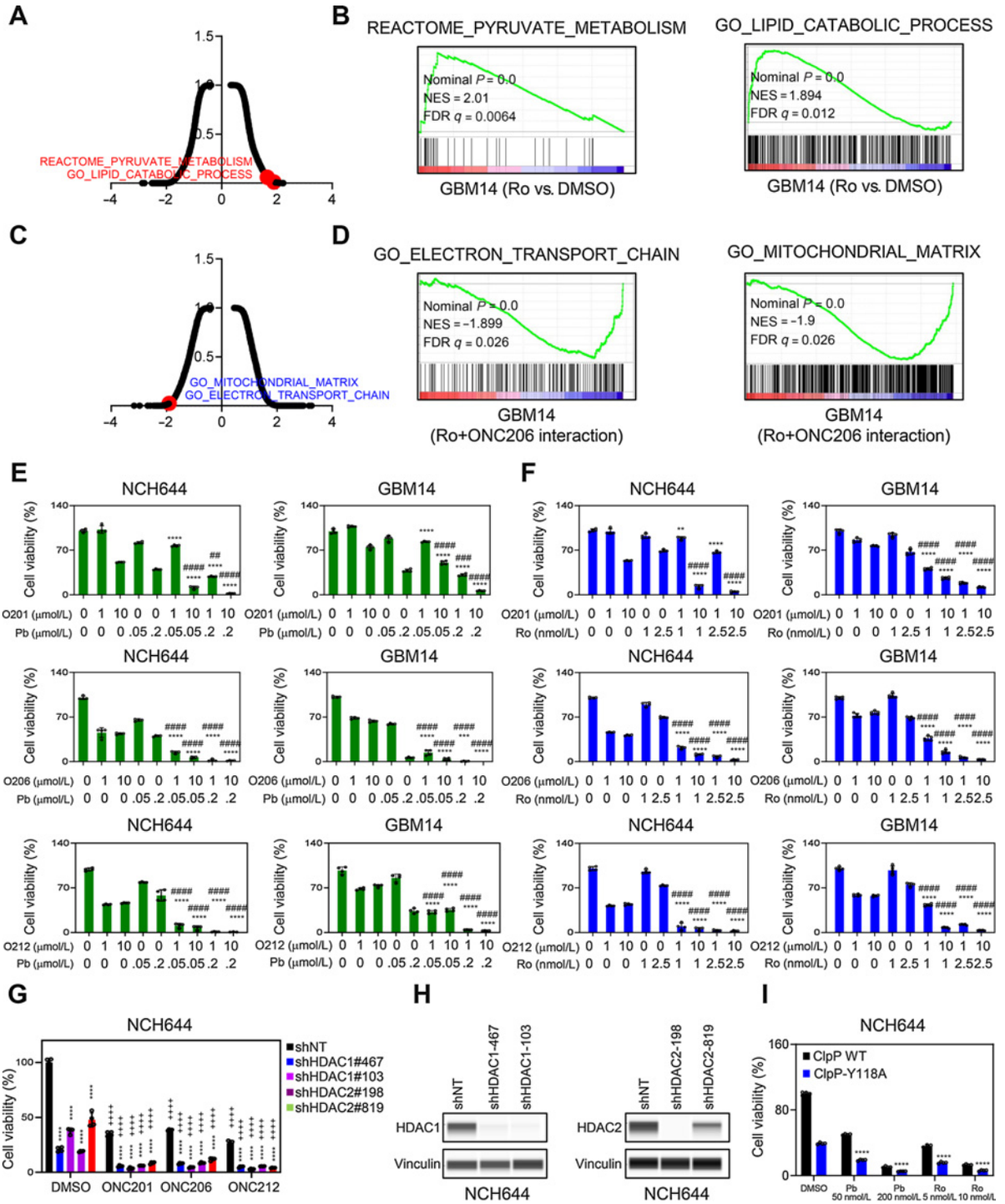

Figure 1.

Activation of the ClpP protease along with inhibition of HDAC1/2 causes synthetic lethality in GBM model systems. **A** and **B,** GBM14 cells were treated with 2.5 nmol/L romidepsin for 24 hours and were submitted for microarray analysis followed by GSEA. Shown in **A** is a volcano plot (FDR-q vs. NES). Highlighted is the NES of Reactome_Pyruvate_Metabolism and Go_Lipid_Catabolic_Process gene sets derived from GSEA. Shown in **B** is the gene set enrichment analysis. NES, normalized enrichment score, FDR-q-value ($n = 2$). **C** and **D,** GBM14 cells were treated with 10 μmol/L ONC206 and 2.5 nmol/L romidepsin for 24 hours and were submitted for microarray analysis followed by GSEA. Shown in **C** is a volcano plot (FDR-q vs. NES). Highlighted is the NES of Go_Mitochondrial_Matrix and Go_Electron_Transport_Chain gene sets derived from GSEA (interaction analysis of the combination treatment). Shown in **D** is the gene set enrichment analysis ($n = 2$). (*Continued on the following page.*)

with vehicle, ONC206, romidepsin, or the combination for 24 hours and thereafter, the individual treatments were analyzed by transcriptome and subsequent gene set enrichment analysis (**Fig. 1A–D**; Supplementary Fig. S1). While romidepsin-treated GBM cells revealed a significant enrichment in metabolic pathways that facilitate an oxidative phenotype, the combination treatment of ONC206 and romidepsin revealed a substantial suppression of gene sets related to the mitochondrial matrix and the electron transport chain, respectively (**Fig. 1A–D**; Supplementary Fig. S1). Following these results, we assessed whether activation of the ClpP protease would synergize with two FDA-approved HDAC inhibitors, to reduce cellular viability (**Fig. 1E** and **F**; Supplementary Figs. S2 and S3). We focused on the established, neurosphere and patient-derived xenograft lines U251, NCH644, GBM14, GBM12, GBM43, and GBM61, respectively. While all imipridones, including ONC201, ONC206, and the latest derivative ONC212, revealed some modest reduction of cellular viability, the addition of either romidepsin or panobinostat led to a synergistic growth reduction in established, neurosphere and patient-derived xenograft cell cultures (**Fig. 1E** and **F**; Supplementary Figs. S2 and S3). The drug combination appeared to be less efficacious in human astrocytes (Supplementary Figs. S2 and S3). We confirmed that our applied drug concentrations are biologically active against their relevant target, revealing that both romidepsin and panobinostat exerted an enhanced acetylation of H3K27, whereas imipridones did not reveal such an effect. Importantly, imipridones did not reverse HDAC inhibitor–mediated hyperacetylation of H3K27 (Supplementary Fig. S4A). Conversely, we validated that imipridones elicited on-target activity by analyzing the protein levels of CLPX. As anticipated, ONC206 potently suppressed the expression levels of CLPX, whereas HDAC inhibitors did not exert a major impact on its expression levels (Supplementary Fig. S4B). Although romidepsin is known to mainly interfere with the function of HDAC1/2, we sought to confirm that indeed the inhibition of those two enzymes is sufficient to elicit a synthetic lethal interaction with activation of the ClpP protease. To this end, we silenced both HDAC1 as well as HDAC2 in NCH644 cells. Thereafter, the GBM cells were treated with ONC201, ONC206, and ONC212 (**Fig. 1G** and **H**). As anticipated, we found that silencing of either HDAC1 or HDAC2 sensitized GBM cells to cytotoxic actions of imipridones (**Fig. 1G** and **H**). In U251 and GBM14 cells, silencing of HDAC1, HDAC2, or the combination by siRNA led to a slight reduction in cellular viability as compared to non-targeting transfected cells (Supplementary Fig. S4C and S4D). In U251 cells, silencing of either HDAC1, HDAC2, or the combination enhanced the efficacy of all three imipridones (Supplementary Figs. S4C). In contrast, in GBM14 cells, while silencing of HDAC1 led to a reduction of viability, interference with HDAC2 demonstrated no impact on cellular growth, indicating different dependencies amongst the two cell cultures. However, dual inhibition of HDAC1 and HDAC2 led to a synergistic reduction in cellular viability in U251 and GBM14 cells. These findings further support the notion that interference with HDAC1, HDAC2, or the combination is sufficient to enhance the efficacy of clinically validated imipridones.

Due to the inherent concern that pharmacological compounds may elicit substantial off-target effects, we extended our analysis, utilizing a constitutively active ClpP mutant (Y118A), which is expected to resemble the on-target effects of imipridones (17). To this purpose, U251 and NCH644 cells were transduced with ClpP wild-type or ClpP-Y118A mutant vector. Established stable clones were treated with romidepsin or panobinstat for 72 hours and cellular viability was assessed thereafter. We found that especially the selective HDAC inhibitor, romidepsin, elicited a reduction of viability more potently in ClpP-Y118A cells as compared to the wild-type ones (**Fig. 1I**; Supplementary Fig. S4E). Similar results were seen when panobinostat was used, albeit not as prominent as with romidepsin. To extend these observations further, we went on to silence HDAC1, HDAC2, or the combination of both in ClpP wild-type and ClpP-Y118A mutant U251 cells and cellular viability was determined (Supplementary Fig. S4F). We found that silencing of both HDAC1 and HDAC2 led to a stronger reduction of cellular viability in ClpP-Y118A mutant cells when compared to the wild-type cells. Notably, the most prominent difference in the reduction of cellular viability between ClpP mutant and wild-type cells was observed in the condition with dual silencing of HDAC1 and HDAC2, consistent with the finding that romidespin (a dual HDAC1 and HDAC2 inhibitor) exerted a more potent reduction of cellular viability in ClpP mutant cells (**Fig. 1I**; Supplementary Fig. S4E and S4F). Thus, these findings establish a novel synthetic lethal interaction between constitutively active ClpP and loss of HDAC1/HDAC2 in GBM model systems, which is translatable through the availability of two classes of clinically validated drugs.

Activation of the ClpP protease along with inhibition of HDAC1/2 activates a cell death with apoptotic features that is partially dependent on caspases

Next, we determined the underlying modality as to how the combination treatment reduced the cellular viability of GBM cells. We hypothesized that based on our microscopic inspection of the GBM cells responding to the drugs this would likely implicate a form of cell death, that is, apoptosis. To this end, we treated NCH644, GBM14, GBM12, GBM61, and U251 cells with vehicle, ONC206, HDAC inhibitor (panobinostat or romidepsin), or the combination of both followed by annexin V/PI staining with subsequent multi-parametric flow cytometry (**Fig. 2A–D**; Supplementary Figs. S5–S7). While ONC206 did not facilitate apoptosis, the combination treatment of either panobinostat+ONC206 or romidepsin+ONC206 led to a significant induction of cell death that was stronger than the treatment with either HDAC inhibitor alone (**Fig. 2A–D**; Supplementary Figs. S5–S7). Similar findings were obtained with ONC201, but higher concentrations were necessary, consistent with its lower potency (Supplementary Fig. S5). In contrast, ONC212 in combination with HDAC inhibitors appeared to have a higher ability to enhance apoptosis for the most part (Supplementary Fig. S7). Given the labeling of the dead cells with annexin, we wondered whether the observed cell death elicited by the combination treatment is dependent on the activation of caspases. To this end, NCH644, GBM14, and U251 GBM

(*Continued.*) **E,** NCH644 and GBM14 cells were treated with ONC201, ONC206, or ONC212 (1 μmol/L and 10 μmol/L) in the presence or absence of panobinostat (50 nmol/L and 200 nmol/L) for 72 hours and cellular viability analysis was performed ($n = 5$). **F,** NCH644 and GBM14 cells were treated with ONC201, ONC206, or ONC212 (1 μmol/L and 10 μmol/L) in the presence or absence of romidepsin (1 nmol/L and 2.5 nmol/L) for 72 hours and cellular viability analysis was performed ($n = 5$). *, The statistical analysis was performed between imipridones and combination treatment. #, The statistical analysis was performed between Pb/Ro and combination treatment. **, $P < 0.01$; $^{***}/^{****}$, $P < 0.001$; $^{\#\#}$, $P < 0.01$; $^{\#\#\#\#}$, $P < 0.001$. **G,** Cellular viability of NCH644 cells transduced with shRNA against HDAC1 or HDAC2 in the presence or absence of ONC201, ONC206, or ONC212 ($n = 4$). *, The statistical analysis was performed between shNT and shHDAC1/2. +, The statistical analysis was performed between imipridones and DMSO treatment. **H,** Protein capillary electrophoresis of NCH644 cells transduced with shRNA against HDAC1 or HDAC2. Vinculin is used as a loading control. **I,** Stable ClpP-wild-type or ClpP-Y118A NCH644 cells were treated with panobinostat/romidepsin for 72 hours and cellular viability analysis was performed ($n = 4$). Statistical significance was assessed ANOVA with Dunnett multiple comparison test in **E–G** and by two-tailed Student *t* test in **I**.

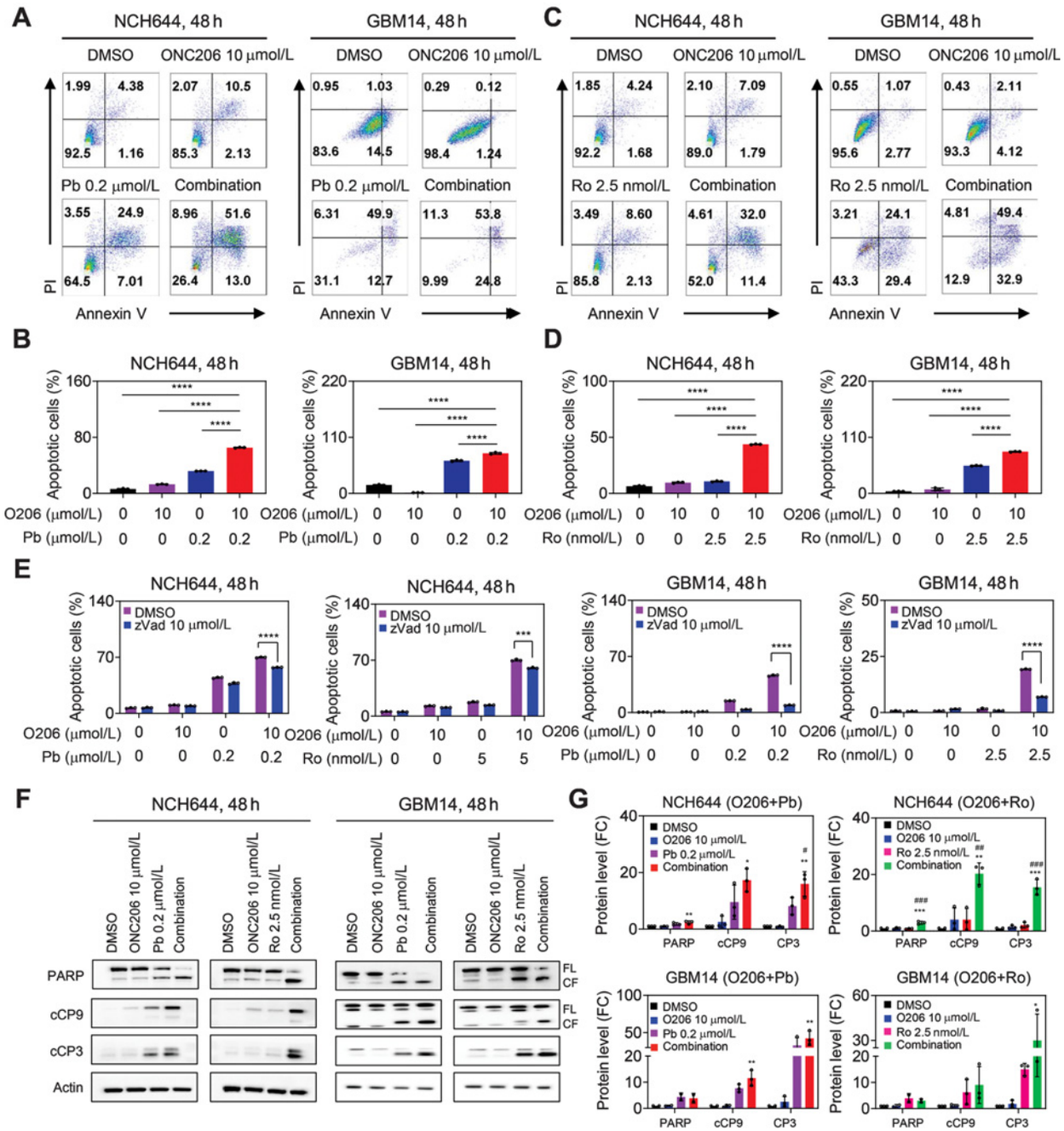

Figure 2.

Activation of the ClpP protease along with inhibition of HDAC1/2 activates a cell death with apoptotic features that is partially caspase dependent. **A** and **B,** NCH644 and GBM14 cells were treated with 10 μmol/L ONC206 and 0.2 μmol/L panobinostat and were labeled with Annexin/PI dye for flow cytometry analysis. The quantification of apoptotic cells is shown in **B** ($n = 3$). **C** and **D,** NCH644 and GBM14 cells were treated with 10 μmol/L ONC206 and 2.5 nmol/L romidepsin and were labeled with Annexin/PI dye for flow cytometry analysis. The quantification of apoptotic cells is shown in **D** ($n = 3$). **E,** NCH644 and GBM14 cells were treated with ONC206 and panobinostat/romidepsin in the presence or absence of 10 μmol/L z-VAD-FMK for 48 hours and were labeled with Annexin/PI dye for flow cytometry analysis. Shown is the quantification of apoptotic cells ($n = 3$). **F** and **G,** NCH644 and GBM14 cells were treated with 10 μmol/L ONC206 and 0.2 μmol/L panobinostat/2.5 nmol/L romidepsin for 48 hours and cell lysates were subjected for standard Western blotting with the indicated antibodies. FL, full length; CF, cleavage fragment. The quantification is shown in **G** ($n = 3$). Statistical significance was assessed ANOVA with Dunnett multiple comparison test. *, The statistic in **G** was compared between imipridones and combination treatment. #, The statistic in **G** was compared between Pb/Ro and combination treatment. *, $P < 0.05$; **, $P < 0.01$; ***, $P < 0.001$; #, $P < 0.05$; ##, $P < 0.01$; ###, $P < 0.001$.

cells were treated with vehicle, ONC206, HDAC inhibitor, or the combination of both in the presence or absence of the pan-caspase inhibitor, zVAD-fmk (**Fig. 2E**; Supplementary Fig. S8A). Indeed, we found that zVAD-fmk led to a partial rescue from cell death induction mediated by either the single treatment with HDAC inhibitors or the combination treatment. To further corroborate the role of caspases, we conducted western blotting analysis of GBM cells treated with vehicle, ONC206, HDAC inhibitors, or the combination of both. We detected an enhanced cleavage of both initiator caspase-9 and effector capase-3 as well as cleavage of PARP upon treatment with the combination treatment (**Fig. 2F** and **G**; Supplementary Fig. S8B and S8C). These results suggest that the combination treatment of HDAC inhibitors and imipridones induces an enhanced cell death with apoptotic features.

Activation of the ClpP protease along with inhibition of HDAC1/2 regulates the expression of antiapoptotic Bcl-2 family members

Apoptotic cell death is regulated at the mitochondrial level by antiapoptotic family members, including Bcl-xL and Mcl-1. Therefore, we analyzed the expression levels of these proteins in the context of single or the combination treatments. We found that the combination treatment of imipridones and HDAC inhibitors led to either a reduction of Mcl-1 protein levels (U251, GBM14, GBM12 cells) or counteracted HDAC inhibitor–mediated increase of Mcl-1 (GBM61 and NCH644 cells; **Fig. 3A** and **B**; Supplementary Fig. S9). There was one exception in the context of the combination treatment of romidepsin and ONC212, involving the GBM12 cells, which did not show a marked reduction of Mcl-1, but instead revealed a reduction in Bcl-xL levels. Concerning Bcl-xL, we found that the combination treatment of panobinostat and ONC206/ONC212 elicited a reduction of Bcl-xL protein levels as well. Similar effects were seen when romidepsin in lieu of panobinostat was used. An exception was noted in the GBM14 cells treated with the combination of imipridone and romidepsin, but instead Mcl-1 protein levels were reduced. In the NCH644 cell line, we found that the combination treatment reduced the levels of Bcl-xL and counteracted HDAC inhibitor–mediated increase of Mcl-1 protein levels (**Fig. 3A** and **B**; Supplementary Fig. S9). These findings suggest a potential role of both Mcl-1 and Bcl-xL in the execution of cell death elicited by the combination treatment, consisting of imipridones and HDAC inhibitors.

In addition, we determined the mRNA expression levels of Mcl-1 and Bcl-xL in U251 and GBM14 cells. Overall, these results showed that the combination treatment led to a reduction of Mcl-1 and Bcl-xL (Supplementary Figs. S10A and S10B). Next, we determined the impact of Mcl-1 and Bcl-xL on the reduction of cellular viability induced by the single and combination treatments by silencing each target with siRNAs (Supplementary Figs. S10C and S10D). While we found a slight enhancement of ONC206-mediated reduction of cellular viability by silencing of Mcl-1 in U251 cells, this effect was not noted in GBM14 cells. Regarding the HDAC inhibitors, we observed a slight to modest enhancement of reduction of cellular viability due to siRNA-mediated suppression of Mcl-1 levels. Notably, the efficacy of the combination treatment of ONC206 and HDAC inhibitors was significantly further enhanced through silencing of Mcl-1 levels, suggesting that the combination treatment (imipridones and HDAC inhibitors) might be more efficacious through the addition of a BH3-mimetic that targets Mcl-1. We continued our analysis with Bcl-xL and did not find any further enhancement of ONC206-mediated reduction of cellular viability when Bcl-xL was silenced under these conditions. Contrasting these results, the efficacy of HDAC inhibitors was enhanced following suppression of Bcl-xL. Notably, the loss of viability elicited by the combination treatment was further increased by silencing of Bcl-xL, suggesting akin to the Mcl-1 silencing experiments the addition of a BH3-mimetic that targets Bcl-xL (e.g., ABT263) may be beneficial (Supplementary Fig. S10C and S10D).

To further support a role for the antiapoptotic Bcl-2 family members in the death elicited by the combination treatment, we ectopically over-expressed Bcl-xL and Mcl-1 by using adenoviruses, which was confirmed by capillary electrophoresis (**Fig. 3C** and **D**; Supplementary Fig. S11). First, we assessed the effect of adenoviral-mediated overexpression of Bcl-xL and Mcl-1 on the combination treatment of ONC206+panobinostat and ONC206+romidepsin in the setting of a cellular viability assay. Our results indicated that forced expression of either Bcl-xL or Mcl-1 mitigated the synergistic reduction of cellular viability elicited by the combination treatment in U251 and GBM14 cells (Supplementary Fig. S11A–S11D). Because Bcl-xL and Mcl-1 are predominantly regulators of cell death, we extended our studies with analysis on apoptotic cell death induction, utilizing annexin V/PI staining followed by multi-parametric flow cytometry (**Fig. 3C** and **D**; Supplementary Fig. S11E–S11G). As anticipated, this analysis provided a clearer picture related to the impact of Bcl-xL and Mcl-1 on cell death induction by the combination treatments (**Fig. 3C** and **D**; Supplementary Fig. S11E–S11G). Importantly, cell death induced by the combination treatment of imipridone and HDAC inhibitors was substantially rescued by Bcl-xL, suggesting that Bcl-xL is a critical mediator of response and resistance to the combination treatment. Mcl-1 overexpression led to a substantial rescue from cell death induced by the combination as well, albeit not as potently. These data suggest that both Mcl-1 and Bcl-xL are implicated in the cell death induced by the combination treatment.

Activation of the ClpP protease along with inhibition of HDAC1/2 affects GBM energy metabolism

Based on our transcriptome and GSEA analyses we continued our studies with extracellular flux analysis to functionally validate these earlier observations. To this end, we used both the U251 and GBM14 cells and treated them with vehicle, romidepsin, ONC206, or combination of both followed by a mitochondrial stress assay on the seahorse analyzer (Supplementary Fig. S12). The seahorse assay determines the baseline OCR and the OCR after sequential addition of oligomycin, the uncoupler FCCP and rotenone/antimycin, which permits the determination of coupled respiration (ATP production from oxidative phosphorylation), maximal respiration and non-mitochondrial respiration. We found that ONC206 reduced the OCR, whereas in contrast HDAC inhibitors led to an inverse response with an increase of the OCR, in keeping with the transcriptome analysis (Supplementary Fig. S12). Earlier findings related to HDAC inhibitors by our group have established that the increase of OCR by HDAC inhibitors represented a pro-survival response (12). Strikingly, the combination treatment of imipridones and HDAC inhibitors led to a substantial reduction of the basal OCR, coupled respiration, and maximal respiration (Supplementary Fig. S12), suggesting that this abrogation of oxidative metabolism might likely be implicated in the therapeutic response by the combination treatment. Moreover, we harnessed the constitutively active ClpP-Y118A mutant in lieu of imipridones and romidepsin. Akin to imipridone treatment, ClpP-Y118A mutant reduced both the OCR and coupled respiration as compared to ClpP wild-type (**Fig. 4A**) and counteracted the increase of OCR elicited by HDAC1/2 inhibition, in keeping with the results related to pharmacologic ClpP activation. Next, we extended these findings related to metabolism by utilizing 13C carbon tracing analysis of uniformly

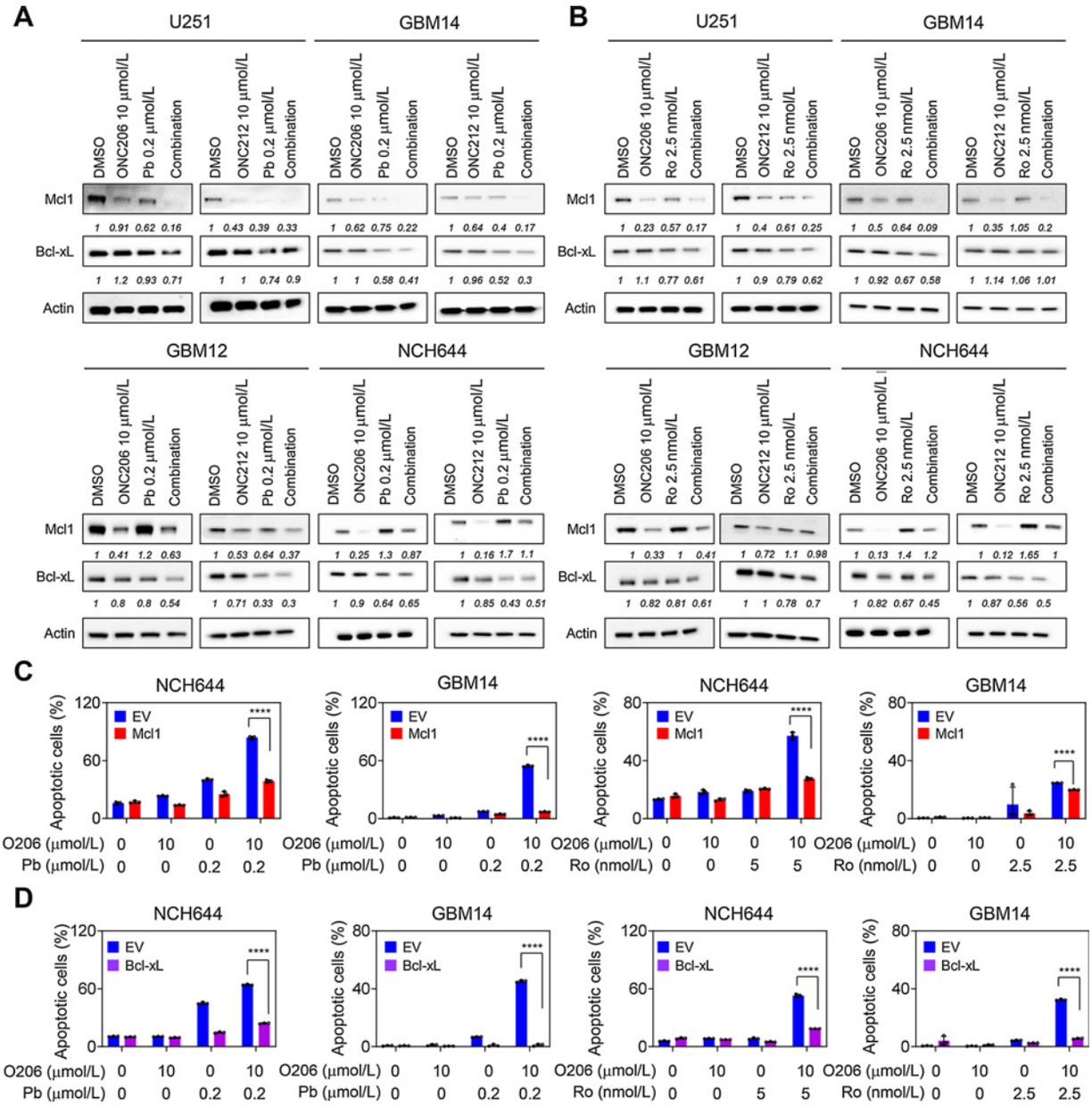

Figure 3.

Activation of the ClpP protease along with inhibition of HDAC1/2 regulates the expression of antiapoptotic Bcl-2 family members. **A** and **B,** Standard Western blots of the antiapoptotic Bcl-2 family members (Mcl-1, Bcl-xL) in U251, GBM14, GBM12, and NCH644 cells treated with 10 μmol/L ONC206/ONC12 and 0.2 μmol/L panobinostat/2.5 nmol/L romidepsin for 24 hours. **C,** NCH644 and GBM14 cells were transduced with empty vector (EV) or Mcl1 adenovirus for 24 hours, treated with 10 μmol/L ONC206 and 0.2 μmol/L panobinostat/2.5 nmol/L romidepsin for 48 hours, and were labeled with Annexin/PI dye for flow cytometry analysis. Shown is the quantification of apoptotic cells ($n = 3$). **D,** NCH644 and GBM14 cells were transduced with empty vector (EV) or Bcl-xL adenovirus for 24 hours, treated with 10 μmol/L ONC206 and 0.2 μmol/L panobinostat/2.5 nmol/L romidepsin for 48 hours, and were labeled with Annexin/PI dye for flow cytometry analysis. Shown is the quantification of apoptotic cells ($n = 3$). Statistical significance was assessed by two-tailed Student t test. ****, $P < 0.001$.

labeled glucose because glucose is known to represent one of the major fuel sources of glioblastoma and other cells (**Fig. 4B–D**). Glucose reacts to pyruvate in glycolysis and in turn is converted to oxaloacetate in the pyruvate carboxylase reaction (biotin dependent CO_2 binding reaction) or oxidized through the multi-enzyme complex pyruvate dehydrogenase (PDH; oxidative decarboxylation dependent on thiamine pyrophosphate; **Fig. 4B**). We hypothesized that following exposure to the combination treatment less glucose carbons would label TCA cycle intermediates based on our findings on the seahorse analyzer. Consistently, we found that both single exposure to imipridones and the combination treatment of ONC206 and romidepsin suppressed labeling of the TCA-cycle metabolites by glucose carbons except for citric acid (**Fig. 4B–D**). All in all, these findings suggest that the combination treatment not

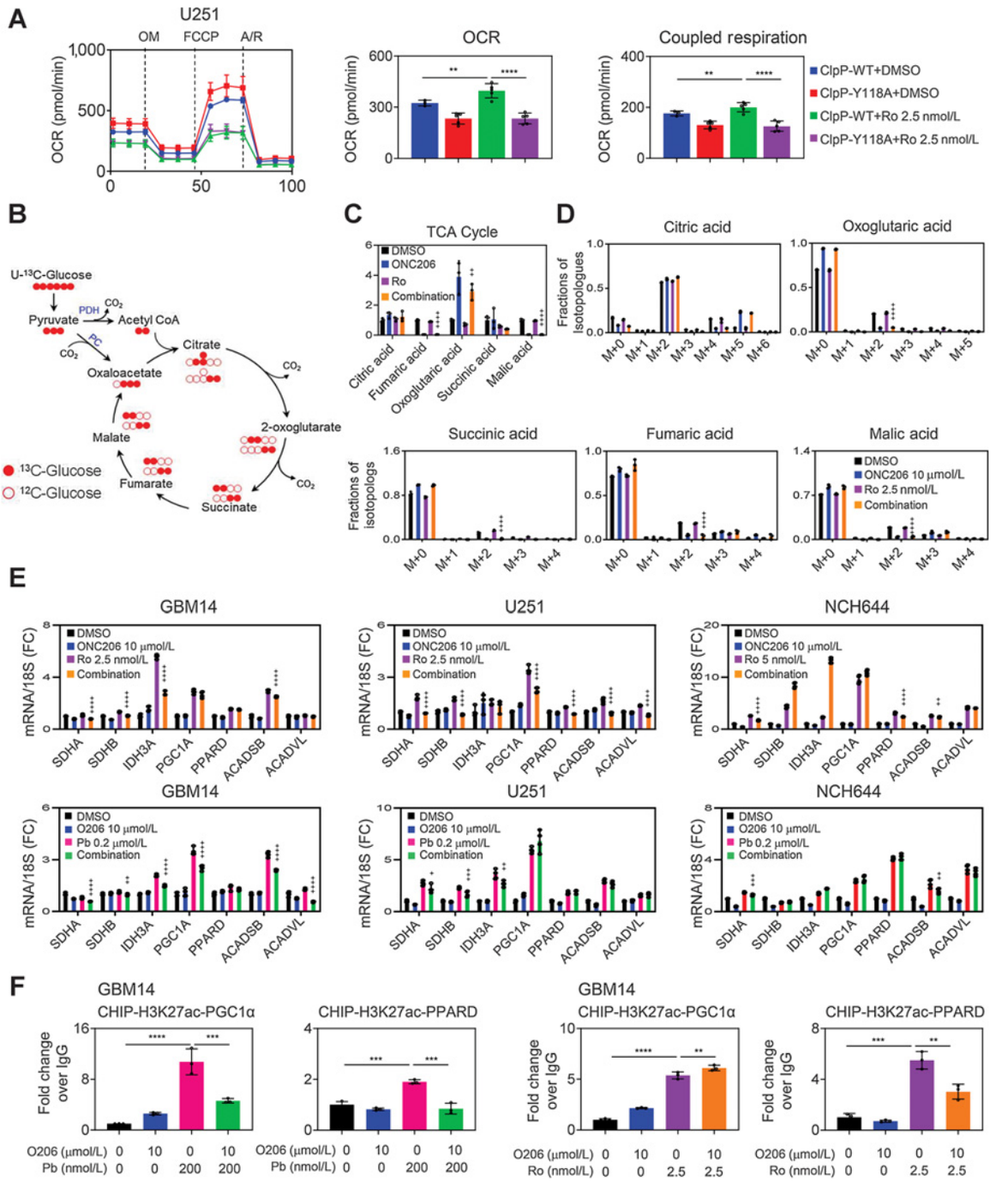

Figure 4.

Activation of the ClpP protease along with inhibition of HDAC1/2 affects GBM energy metabolism. **A,** Stable ClpP-wild type or ClpP-Y118A U251 cells were treated with 2.5 nmol/L romidepsin for 72 hours and analyzed for OCR by a mito stress assay on a Seahorse XFe24 device. F, FCCP; OM, oligomycin; R/A, rotenone/antimycin. The graph (right) shows the OCR and coupled respiration level ($n = 4$–5). **B,** The graphic presents one turn of the TCA cycle. Glucose is metabolized to pyruvic acid (m+3; three carbons labeled). When glucose is oxidized in the TCA cycle, citric acid (m+2) is produced (two carbons are labeled). When glucose is used for anaplerosis, citric acid (m+3) is produced (three carbons are labeled). **C** and **D,** GBM14 cells were incubated in DMEM (devoid of phenol red, pyruvate and glutamine) supplemented with 25 mmol/L U-^{13}C-glucose, 4 mmol/L glutamine, and 1.5% dialyzed FBS in the presence of 10 μmol/L ONC206, 2.5 nmol/L romidepsin or the combination for 24 hours. Shown are the total metabolites in the TCA cycle in **C** and the fractions of isotopologs in **D** ($n = 3$). **E,** Real-time PCR analysis of GBM14, U251, and NCH644 cells treated with 10 μmol/L ONC206, 2.5 nmol/L romidepsin/0.2 μmol/L panobinostat, or the combination for 24 hours. 18S is used as an internal control. Shown are means and SD ($n = 4$). **F,** CHIP-qPCR with anti-H3K27ac antibody of two different promoter regions (PGC1α and PPARD) in GBM14 treated with ONC206, 0.2 μmol/L panobinostat/2.5 nmol/L romidepsin, or the combination for 24 hours ($n = 3$). Statistical significance was assessed ANOVA with Dunnett multiple comparison test. **, $P < 0.01$; ***/****, $P < 0.001$. +, The statistic in **D** and **E** was compared between Pb/Ro and combination treatment.

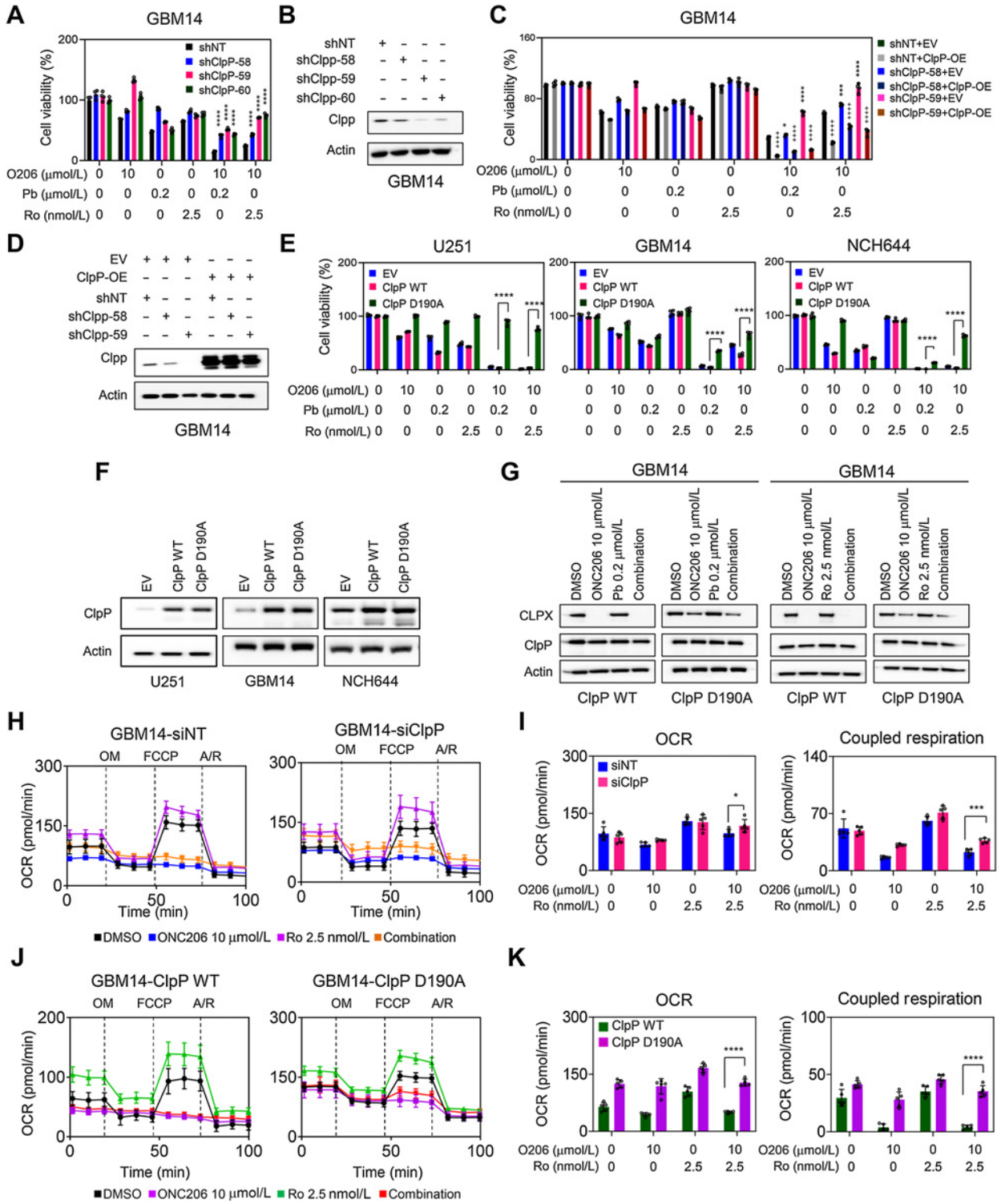

Figure 5.

The combination treatment of imipridones along with HDAC inhibitors is highly dependent on mitochondrial ClpP. **A,** GBM14 cells were transduced with three different shRNA against CLPP, were treated with 10 μmol/L ONC206 and 0.2 μmol/L panobinostat/2.5 nmol/L romidepsin for 72 hours, and cellular viability analysis was performed ($n = 4$). **B,** Standard Western blots of GBM14 transduced with three different shRNA against ClpP. Actin is used as a loading control. **C,** Stable shCLPP GBM14 cells were transduced with empty vector (EV) or an adenovirus carrying CLPP cDNA for 24 hours (CLPP-OE), were treated with 10 μmol/L ONC206 and 0.2 μmol/L panobinostat/2.5 nmol/L romidepsin for 72 hours, and cellular viability analysis was performed ($n = 4$). Statistical significance was assessed ANOVA with Dunnett multiple comparison test in **A** and **C**. *, The statistical analysis was performed between shNT and shClpP. +, The statistical analysis was performed between empty vector (EV) and ClpP-OE. (*Continued on the following page.*)

only impairs general oxidative metabolism, but more specifically it interferes with glucose oxidation.

Given the impact on oxidative metabolism by the various treatments, we followed up with protein expression analysis of the different complexes that make up the respiratory chain in mitochondria (Supplementary Figs. S13A and S13B). We found that predominantly imipridones suppressed the expression of respiratory complexes, whereas for the most part HDAC inhibitors led to an increase. The combination treatment mediated a substantial suppression of most components of the respiratory chain, in keeping with the results obtained from the seahorse analyzer and the glucose 13C tracing experiments (**Fig. 4B**–**D**). Next, we assessed several key genes that encode for pivotal factors, involved in oxidative energy metabolism, including enzymes, and transcription factors that are known to drive OXPHOS-dependent energy metabolism (**Fig. 4E**). We found that HDAC inhibitors increased the mRNA levels of SDHA and SDHB, which are part of complex II of the respiratory chain. In addition, we noted an increase of IDH3A as well as ACADSB and ACADVL (**Fig. 4E**). Importantly, two transcription factors, PGC1A and PPARD that are known to facilitate oxidative energy metabolism were increased as well. In some instances, HDAC inhibitor–mediated increase of these mRNAs was counteracted by imipridones, in keeping with our transcriptome and gene set enrichment analysis and the measurements on the seahorse analyzer. Next, we investigated the mechanism by which HDAC inhibitors facilitate up-regulation of oxidative metabolism. We hypothesized that HDAC inhibitors would facilitate the presence of active histone marks in the promoter region of these genes. Following treatment with vehicle, imipridones, HDAC inhibitors, or the combination of both, we performed chromatin immunoprecipitation with an antibody against H3K27ac and analyzed the promoter regions of PGC1A, PPARD, and ACADSB by real-time PCR analysis. As anticipated, we found that HDAC inhibitors increased the presence of H3K27ac at the promoter regions of these genes in both U251 and GBM14 cells (**Fig. 4F**; Supplementary Fig. S13C and S13D). It is noteworthy that the combination treatment counteracted this increase only in some, but not all promoter regions, suggesting that the combination treatment reversed HDAC inhibitor–mediated activation of oxidative metabolism at least in part independent of the epigenome and transcriptome.

The combination treatment of imipridones along with HDAC inhibitors is highly dependent on the mitochondrial ClpP protease

Next, we sought to establish further mechanisms through which the combination treatment elicited killing of GBM cells and regulated energy metabolism. To this end, we hypothesized that the ClpP protease is likely involved in this process. We silenced the expression of the ClpP protease by both siRNA and shRNAs in GBM cells followed by treatment with ONC206 and ONC212 (**Fig. 5A** and **B**; Supplementary Fig. S14). We found that silencing of ClpP attenuated the reduction in viability caused by imipridones, in keeping with the notion that the ClpP protease represents the primary target of both ONC206 and ONC212 (Supplementary Fig. S14A–S14C). Next, we extended these findings to the combination treatments (Supplementary Fig. S14D). To this end, both U251 and GBM14 cells were treated with imipridones (ONC201, ONC206, or ONC212), HDAC inhibitors (panobinostat or romidepsin), or the respective combination treatment and analyzed for cellular viability. As anticipated, we noted a rescue from imipridone-mediated reduction in cellular viability (**Fig. 5A** and **B**; Supplementary Fig. S14D). To ensure specificity of these findings, we performed a cDNA rescue experiment, utilizing an adenoviral vector encoding murine ClpP (**Fig. 5C** and **D**). We found that adenoviral-mediated over-expression of ClpP cDNA reversed the ClpP shRNA-driven rescue from the reduction of cellular viability by the combination treatment (**Fig. 5C** and **D**). Next, we assessed whether silencing of ClpP would also rescue from the cell death induced by the combination treatment. To this purpose, ClpP and non-targeting siRNA-transfected U251 cells were treated with vehicle, ONC206, HDAC inhibitors, or the respective combinations followed by annexin V/PI staining analyzed by multi-parametric flow cytometry (Supplementary Figs. S15A–S15C). Our results showed that silencing of ClpP by siRNA rescued from cell death induced by the combination treatment, albeit this effect was less pronounced as compared to the measurements obtained in the cell viability assay, suggesting that the activity of the ClpP protease may be more important for the inhibition of proliferation mediated by the combination treatment than for cell death induction. In alignment with these findings, we found that silencing of ClpP protected from imipridone-mediated suppression of CLPX protein levels (Supplementary Fig. S15D). Next, we assessed the impact of the ClpP (D190A) mutant on the reduction of cellular viability imposed by single treatment with ONC206 or the combination treatment of imipridone and HDAC inhibitors. We found that ClpP-D190A rescued the reduction of viability induced by ONC206 as well as the combination treatment of ONC206 and HDAC inhibitors in U251, GBM14, and NCH644 GBM cells (**Fig. 5E** and **F**), lending significant specificity to our findings and suggesting broad applicability. Similarly, CLPX protein levels were maintained in the presence of mutant ClpP-D190A following treatment with ONC206 (**Fig. 5G**; Supplementary Fig. S15E).

Next, we transfected U251 and GBM14 cells with non-targeting or ClpP siRNA and treated them with vehicle, ONC206, HDAC inhibitors, or the respective combination treatments. Thereafter, we performed extracellular flux analysis in the context of a mitochondrial stress assay (**Fig. 5H** and **I**; Supplementary Fig. S16A and S16B). We found that imipridone-mediated reduction in OCR and coupled respiration (ATP production) was rescued by silencing of the ClpP protease. To further extend the specificity of these findings, we utilized a ClpP-D190A mutant. U251 GBM cells were transduced with lentiviral particles encoding for ClpP wild-type or ClpP-D190A mutant (**Fig. 5J** and **K**; Supplementary Fig. S16C–S16F). Following selection,

(*Continued.*) **D,** Standard Western blots of stable shCLPP GBM14 cells were transduced with empty vector (EV) or adenovirus (CLPP-OE) for 24 hours. **E,** U251, GBM14, and NCH644 cells were transduced with empty vector (EV), ClpP wild-type, or ClpP D190A lentiviral particles and were treated with 10 μmol/L ONC206, 0.2 μmol/L panobinostat/2.5 nmol/L romidepsin, or the combination for 72 hours and cellular viability analysis was performed ($n = 4$). **F,** Standard Western blot of U251, GBM14, and NCH644 cells transduced with empty vector (EV), ClpP wild-type, or ClpP D190A lentiviral particles. **G,** Standard Western blot of GBM14 cells transduced with ClpP wild-type or ClpP D190A lentiviral particles and were treated with 10 μmol/L ONC206, 0.2 μmol/L panobinostat/2.5 nmol/L romidepsin, or the combination for 24 hours. **H** and **I,** GBM14 cells were transfected with siRNA against CLPP; treated with 10 μmol/L ONC206, 2.5 nmol/L romidepsin, or the combination of both for 24 hours; and analyzed for OCR by a mito stress assay on a Seahorse XFe24 device. F, FCCP; OM, oligomycin; R/A, rotenone/antimycin. The graph in **I** shows the OCR and coupled respiration level ($n = 4$–5). **J** and **K,** Stably transduced cells expressing ClpP wild-type or ClpP D190A treated with 10 μmol/L ONC206, 2.5 nmol/L romidepsin, or the combination of both for 24 hours were analyzed for OCR by mito stress assay on a Seahorse XFe24 device. The graph in **K** show the OCR and coupled respiration level ($n = 5$). Statistical significance was assessed by two-tailed Student *t* test in **E**, **I**, and **K**. *, $P < 0.05$; ***/****, $P < 0.001$.

these cells were subjected to treatments with ONC206, HDAC inhibitors (romidepsin or panobinostat), and the respective combinations followed by extracellular flux analysis. We found that ClpP-D190A mutant rescued from ONC206 or ONC206+HDAC inhibitor–mediated reduction in OCR as well as coupled respiration (ATP production; **Fig. 5J** and **K**; Supplementary Fig. S16C–S16F). Moreover, ClpP-D190A reversed imipridone and combination treatment-mediated suppression of respiratory complexes (Supplementary Fig. S16G). Consistently, our tracing analysis revealed that less glucose carbons are utilized for the synthesis of both AMP and ATP following treatment with imipridones or the combination treatments (Supplementary Fig. S17A). Considering our transcriptomic and metabolic observation there appears a reasonable likelihood that parts of the reduction of the combination treatment is dependent on ATP since aside from glycolysis, oxidative phosphorylation, and the TCA-cycle are the main drivers of ATP production. To test this idea further, we treated U251 and GBM14 cells with vehicle, ONC206, HDAC inhibitors, or combination treatments of ONC206 and HDAC inhibitors in the presence or absence of ATP. We found that ATP partially reversed the reduction in cellular viability driven by the combination treatment, suggesting that energy deprivation related to stalling of oxidative metabolism with subsequent reduction of ATP is a driver of the efficacy of the combination treatment (Supplementary Fig. S17B). Furthermore, we determined how the ClpP-D190A mutation affects the Bcl-2 family of proteins following treatment with imipridones, HDAC inhibitors, and the combination of both (Supplementary Fig. S17C). We found that ClpP-D190A mutation rescued from ONC206 or ONC206+HDAC inhibitor–mediated reduction of Mcl-1 protein levels (Supplementary Fig. S17C).

Combined treatment with imipridones and HDAC inhibitors elicits enhanced antiglioma activity in PDX models

We followed up with *in vivo* studies related to the various treatments. To this end, we utilized patient-derived xenograft models and initiated our studies with two well-characterized PDX GBM models (GBM12 and GBM43) to study the growth of subcutaneous tumors following treatment with vehicle, ONC206, romidepsin, and the combination treatment followed by toxicity analysis (**Fig. 6A–D**). Following establishment of tumors, the animals received treatment with the indicated compounds and regular size measurements were performed. While ONC206 had fairly little impact on the growth of the GBM12 and GBM43 xenografts, we noted a substantial tumor size reduction after treatment with the selective HDAC1/2 inhibitor, romidepsin (**Fig. 6A–D**). Notably, the combination treatment reduced the tumor size further as compared to both single treatments, in keeping with our observations in the *in vitro* setting. It is noteworthy that this effect was not accompanied by organ toxicity (Supplementary Fig. S18A). Next, we investigated how the different treatments affected the histology of the tumors (**Fig. 6E–G**). Standard H&E morphology demonstrated a potent reduction in cellularity following exposure to the combination treatment, which was more significant than following treatment with romidepsin alone. To account for cell death induction, we followed up with TUNEL staining and found that there was significant DNA fragmentation in the tumors exposed to the combination treatment (higher magnification of the same image is shown in the supplement to emphasize the nuclear staining; **Fig. 6F**; Supplementary Fig. S18C). To account for cellular proliferation, the slides from the different groups were labeled with an antibody against Ki-67 (**Fig. 6G**). We found that romidepsin reduced the number of positive nuclei, which was further reduced by the combination treatment. Thus, the combination treatment exerted its effects in part through suppression of proliferation and induction of cell death, in keeping with the findings observed *in vitro*.

Next, we assessed the efficacy of the drug combination of imipridones and HDAC inhibitors in an orthotopic GBM12 PDX model. We utilized panobinostat since this compound has been shown to penetrate the blood–brain barrier and appeared to be efficacious in a model system of midline glioma, harboring the H3K27M mutation (25). ONC212 was employed in the orthotopic model because previous research revealed that ONC212 exerted some single-agent efficacy in PDX GBM model systems (16). While the single treatment exerted no survival benefit, we found that the combination treatment of ONC212 and panobinostat led to a significant extension of animal survival (**Fig. 6H–J**). In addition, we used the GL261 murine model since it has an active immune system to closely mirror the brain microenvironment. Following injection of GL261 cells and establishment of tumors, four treatment groups were formed, consisting of vehicle, ONC212, panobinostat, and the corresponding combination treatment (**Fig. 6K–M**). While single treatment did not increase the survival of host animals, we found that the combination treatment significantly extended overall survival compared to the vehicle-treated animals (**Fig. 6K–M**) and no organ toxicity was observed on the basis of the histologic analysis (Supplementary Fig. S18B).

Discussion

Recent evidence from the literature highlights that GBMs display critical metabolic dependencies, including carbohydrate, amino acid, and fatty acid metabolism (4, 26–29). In agreement with the transcriptional and proteomic heterogeneity of these recalcitrant tumors, it recently became apparent that these tumors have a central core that relies mostly on glycolysis, which is surrounded by a periphery that appears to be dependent on oxidative metabolism, for example, beta-oxidation of fatty acids (30). These observations imply that targeting different metabolic regions within glial tumors may be a viable therapeutic approach. While these metabolic changes mentioned above are associated with a particular location in a tumor, drug-induced metabolic reprogramming adds another layer of complexity to this scenario. In this vein, several recent reports suggest that there may be substantial therapeutic benefits to interfere with drug-induced metabolic reprogramming. For instance, melanomas harboring the BRAF V600E mutation that were treated with vemurafenib developed reliance on oxidative energy metabolism. In turn, inhibitors of oxidative phosphorylation acted synergistically with BRAF inhibitors to reduce the viability of melanoma cells and xenografts (31). While it seems that a significant number of tumors respond to treatment with transitioning their metabolism to become strongly dependent on oxidative phosphorylation, there are pertinent examples in the literature that render cancer cells more reliant on glycolysis and the pentose phosphate pathway. For instance, such findings were observed in preclinical models of pancreatic carcinoma that were exposed to the FDA-approved drug gemcitabine (32). These earlier observations in other tumor entities suggest that targeting drug-induced metabolic reprogramming may become a rising strategy for the treatment of hematological and solid malignancies. However, this concept has not been explored in depth in brain tumors, especially in GBM. Therefore, additional studies are necessary to clarify whether drug-induced reprogrammed metabolism is a worthwhile target in GBM.

In this report, we made the discovery that in glioblastoma model systems specific activation of the ClpP protease (Y118A) is synthetically lethal with either HDAC1 or HDAC2 inhibition by inducing intrinsic apoptosis relying on both anti-apoptotic Bcl-xL and Mcl-1.

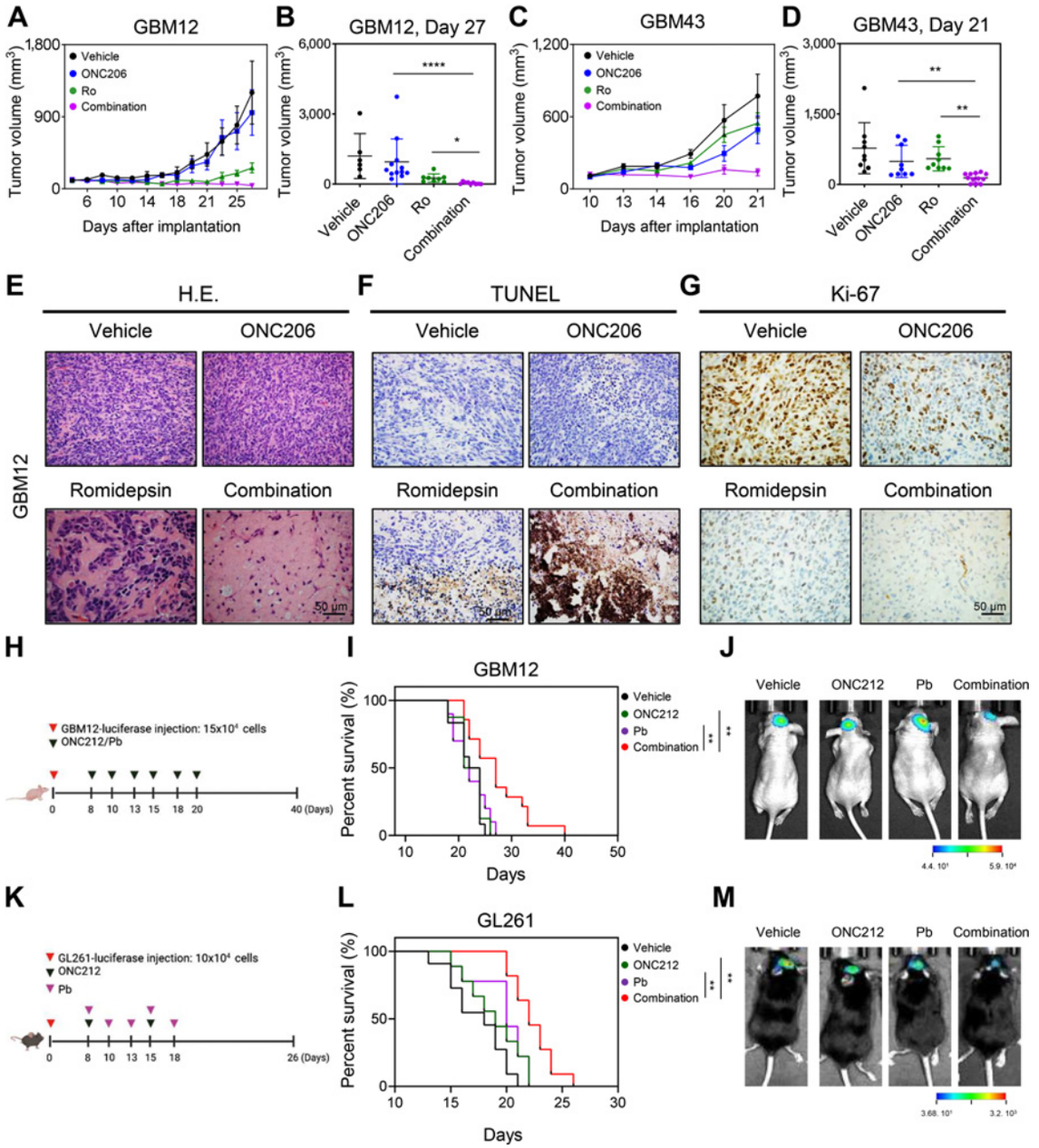

Figure 6.

Combined treatment with imipridones and HDAC inhibitors elicits enhanced antiglioma activity in PDX models**. A–D,** GBM12 and GBM43 cells were implanted into the subcutis of immunocompromised Nu/Nu mice and were treated with vehicle, ONC206 (50 mg/kg), romidepsin (0.5 mg/kg), or combination treatment of both three times per week after tumors were established. The tumor volumes over time are shown in **A** and **C** and the tumor volumes on the last day of the experiment are shown in **B** and **D**. **E–G,** Tumors from the experiment in **A** were fixed and stained with H&E, TUNEL, or Ki-67. **H–J,** Survival analysis of immunocompromised Nu/Nu mice implanted with GBM12-luc 15 × 10^4 cells and administered with vehicle, ONC212 (50 mg/kg), panobinostat (5 mg/kg), or combination treatment of both two times per week after 8 days post intracranial. The log-rank test was used to assess statistical significance (vehicle $n = 12$, ONC212 $n = 8$, Pb $n = 10$, and combination $n = 14$). The representative IVIS image from each group after 22 days of implantation was shown in **J**. **K–M,** Survival analysis of C57BL/6NTac mice implanted with GL261-luc 10×10^4 cells and administered with vehicle, ONC212 (50 mg/kg), panobinostat (5 mg/kg), or combination treatment of both two times per week for panobinostat and one time per week for ONC212 after 8 days post intracranial. The log-rank test was used to assess statistical significance (vehicle $n = 11$, ONC212 $n = 9$, Pb $n = 9$, and combination $n = 11$). The representative IVIS image from each group after 17 days of implantation is shown in **M**. Scale bar, 50 μm. Statistical significance was assessed ANOVA with Dunnett multiple comparison test.

These findings are timely and suggest that FDA-approved drugs, that is, panobinostat, may be effectively combined with clinically validated imipridones, such as ONC201 or the more recently developed compounds, ONC206 and ONC212. We confirmed this notion by testing these drug combinations in a range of different highly biologically relevant models of human GBMs, including PDX models *in vitro* and most relevantly *in vivo*. Although our experiments confirm on-target efficacy (HDAC1/2 and CLPP) we cannot completely exclude that there are off-target effects elicited by the combination treatment. Since we observed an extension of overall survival by the combination treatment in two orthotopic mouse models, it is conceivable that temozolomide and/or radiation will likely further enhance the efficacy of this treatment regimen, encouraging the launch of potential phase I clinical trials. Transcriptome and metabolite tracing analysis pinpointed that this combination treatment exerts its effect in part through blocking oxidative energy metabolism in a manner highly dependent on the ClpP protease since a ClpP-D190A mutant abrogated the killing effects and the metabolic effects of the combination treatment. This finding is relevant since not long ago there was some controversy about the direct target of imipridones. Initially, these compounds were identified as potent inducers of the death ligand TRAIL (13, 14, 16, 33), but shortly thereafter it became clear that imipridones (i.e., ONC201) appeared to exert their anti-tumor effects through other means as well, such as inhibition of proliferation or modulation of intrinsic apoptosis (i.e., Mcl-1 suppression; ref. 34). In this context, it was shown that these compounds induce the integrated stress response with a prominent increase in ATF4. In addition, dopamine receptors were identified as targets for imipridones (35). Consistently, high levels of dopamine receptors (DRD2) conferred increased susceptibility of cancer cells to the cytotoxic effects of imipridones (35). Our research has shown that MYC expression levels may be predictive of a potentially more pronounced response to imipridones (16). We and others were also able to link imipridones to mitochondrial energy metabolism since ONC201 and more potently ONC206 and ONC212 interfered with OCR, mitochondrial respiration, and coupled respiration (16). Imipridones also modulated glycolysis in a cell type and context-dependent manner (16). Given their primary impact on oxidative metabolism it was not surprising that blockage of glycolysis by 2-DG enhanced the potency of ONC201 in several model systems of human GBMs (36). Along with the inhibition of tumor energy metabolism there was an activation of the serine-glycine synthesis pathway with induction of PHGDH, PSAT1, and PSPH, which was partially orchestrated by imipridone-mediated increase of ATF4 (16, 36). More recently, two groups identified ClpP as a novel target for imipridones and linked the ClpP protease with tumor respiration and oxidative phosphorylation (15, 17–19). However, these studies were limited and did not involve a larger group of different cell lines, that is, there were no prior studies on GBM PDX or neurosphere models that would inform about the importance of ClpP as the actual target of imipridones in those sets of models. Moreover, since single treatments are most likely to fall behind expectations, it is highly critical to determine the role of ClpP in drug combinations, involving standard and novel engineered/chemically modified imipridones. In this context, the present study significantly extends prior knowledge since it demonstrates for the very first time that imipridone-containing drug combinations require a functional mitochondrial ClpP protease protein. We confirmed this critical notion through a two-prong strategy, involving silencing experiments and more importantly a point mutation in ClpP, which has been shown to arise in contexts of imipridone-induced secondary resistance (evolving from prior treatments; ref. 17). These findings are unfortunate to some extend since it might suggest that the present combination treatment of imipridone and HDAC inhibitors may not overcome secondary imipridone resistance mediated by certain ClpP point mutations. However, it is still possible that the present combination will be effective to overcome other forms of imipridone-mediated resistance. Another critical aspect is whether the combination treatment of imipridones and HDAC inhibitors would prevent the occurrence of a secondary ClpP-D190A mutation, which may be part of future investigations. Our finding that imipridones and HDAC inhibitors appear to exert their anti-glioma effects to a significant degree through blockage of oxidative energy metabolism is novel and it seems likely that the metabolic stress induced by the combination treatment is upstream of intrinsic apoptosis. Mechanistically, HDAC inhibitors and imipridones exert opposite effects on oxidative metabolism, whereby HDAC inhibitors drive and imipridones block tumor cell respiration. While HDAC inhibitors transcriptionally up-regulate enzymes and transcription factors that facilitate oxidative metabolism, imipridones suppress the expression of respiratory complexes in a manner largely dependent on the ClpP protease.

In summary, we have unraveled a novel synthetic lethal interaction, involving HDAC1 and HDAC2 and the mitochondrial ClpP protease, which exerts its effects in part through suppression of tumor cell metabolism. Therefore, HDAC inhibitors may be effectively combined with imipridones in GBM.

Authors' Disclosures

S. Schiffgens reports grants from Fritz-Thyssen-Foundation during the conduct of the study. H.O. Akman reports grants from Department of Defense and NIH, R01, as well as other support from Keith B Hayes Foundation and Gayle Lipsig outside the submitted work. V.V. Prabhu reports other support from Oncoceutics/Chimerix during the conduct of the study; in addition, V.V. Prabhu has a patent for Imipridones for gliomas (US10172862B2) issued and a patent for G protein-coupled receptor (GPCR) modulation by imipridones (US11116771B2) issued. J.E. Allen reports personal fees, non-financial support, and other support from Chimerix and Oncoceutics during the conduct of the study, as well as other support from University of Pennsylvania and Pennsylvania State University outside the submitted work; in addition, J.E. Allen has a patent for ONC201 and other imipridones pending, issued, and with royalties paid from Oncoceutics/Chimerix. No disclosures were reported by the other authors.

Authors' Contributions

T.T.T. Nguyen: Conceptualization, formal analysis, investigation, writing–review and editing. **E. Shang:** Investigation. **S. Schiffgens:** Investigation. **C. Torrini:** Investigation. **C. Shu:** Investigation. **H.O. Akman:** Resources. **V.V. Prabhu:** Resources, writing–review and editing. **J.E. Allen:** Resources, writing–review and editing. **M.-A. Westhoff:** Writing–review and editing. **G. Karpel-Massler:** Writing–review and editing. **M.D. Siegelin:** Conceptualization, supervision, investigation, methodology, writing–original draft, writing–review and editing.

Acknowledgments

We thank Dr. Elena Bianchetti for her outstanding technical assistance. These studies used the resources of the Cancer Center Flow Core Facility funded in part through center grant P30CA013696 and S10RR027050. Transcriptome analysis was supported by the CTSA grant UL1-TR001430 to the Boston University Microarray and Sequencing Resource Core Facility. The studies presented in this work were carried out in part in the Oncology Precision Therapeutics and Imaging Core (OPTIC) Shared Resource at Columbia University Herbert Irving Comprehensive Cancer Center, which is partially funded by the Columbia University Medical Center Cancer Support Grant [NIH grant #P30 CA013696 (National Cancer Institute)]. The authors wish to thank Wendi Liu and Christopher Damoci for study design, execution, and assistance in IVIS Spectrum Optical Imaging System (PerkinElmer). This work was supported in part by grants from M.D. Siegelin: NIH NINDS R01NS095848, R01NS102366, R01NS113793; Louis V. Gerstner, Jr. Scholars Program (2017–2020); American

Brain Tumor Association Discovery Grant 2017 (DG1700013); Schaefer Research Scholars Program Awards 2020; and American Brain Tumor Association Discovery Grant Supported by Sontag Foundation 2021 (DG2100041). T.T.T. Nguyen: American Brain Tumor Association Basic Research Fellowship in Memory of Katie Monson (BRF1900018). S. Schiffgens: Fritz Thyssen Foundation (40.19.0.016MN).

The costs of publication of this article were defrayed in part by the payment of page charges. This article must therefore be hereby marked *advertisement* in accordance with 18 U.S.C. Section 1734 solely to indicate this fact.

Received August 5, 2021; revised December 28, 2021; accepted February 16, 2022; published first February 22, 2022.

References

1. Wang LB, Karpova A, Gritsenko MA, Kyle JE, Cao S, Li Y, et al. Proteogenomic and metabolomic characterization of human glioblastoma. Cancer Cell 2021;39:509–28.
2. Garofano L, Migliozzi S, Oh YT, D'Angelo F, Najac RD, Ko A, et al. Pathway-based classification of glioblastoma uncovers a mitochondrial subtype with therapeutic vulnerabilities. Nat Cancer 2021;2:141–56.
3. Darmanis S, Sloan SA, Croote D, Mignardi M, Chernikova S, Samghababi P, et al. Single-cell RNA-seq analysis of infiltrating neoplastic cells at the migrating front of human glioblastoma. Cell Rep 2017;21:1399–410.
4. Guo D, Reinitz F, Youssef M, Hong C, Nathanson D, Akhavan D, et al. An LXR agonist promotes glioblastoma cell death through inhibition of an EGFR/AKT/SREBP-1/LDLR-dependent pathway. Cancer Discov 2011;1:442–56.
5. Eleutherakis-Papaiakovou E, Kanellias N, Kastritis E, Gavriatopoulou M, Terpos E, Dimopoulos MA. Efficacy of panobinostat for the treatment of multiple myeloma. J Oncol 2020;2020:7131802.
6. Wang J, Jiang J, Chen H, Wang L, Guo H, Yang L, et al. FDA-approved drug screen identifies proteasome as a synthetic lethal target in MYC-driven neuroblastoma. Oncogene 2019;38:6737–51.
7. Gryder BE, Wu L, Woldemichael GM, Pomella S, Quinn TR, Park PMC, et al. Chemical genomics reveals histone deacetylases are required for core regulatory transcription. Nat Commun 2019;10:3004.
8. Zhang Y, Ishida CT, Ishida W, Lo SL, Zhao J, Shu C, et al. Combined HDAC and bromodomain protein inhibition reprograms tumor cell metabolism and elicits synthetic lethality in glioblastoma. Clin Cancer Res 2018;24:3941–54.
9. Sanchez GJ, Richmond PA, Bunker EN, Karman SS, Azofeifa J, Garnett AT, et al. Genome-wide dose-dependent inhibition of histone deacetylases studies reveal their roles in enhancer remodeling and suppression of oncogenic super-enhancers. Nucleic Acids Res 2018;46:1756–76.
10. Nagaraja S, Vitanza NA, Woo PJ, Taylor KR, Liu F, Zhang L, et al. Transcriptional dependencies in diffuse intrinsic pontine glioma. Cancer Cell 2017;31:635–52.
11. Mazzone R, Zwergel C, Mai A, Valente S. Epi-drugs in combination with immunotherapy: a new avenue to improve anticancer efficacy. Clin Epigenetics 2017;9:59.
12. Nguyen TTT, Zhang Y, Shang E, Shu C, Torrini C, Zhao J, et al. HDAC inhibitors elicit metabolic reprogramming by targeting super-enhancers in glioblastoma models. J Clin Invest 2020;130:3699–716.
13. Wagner J, Kline CL, Pottorf RS, Nallaganchu BR, Olson GL, Dicker DT, et al. The angular structure of ONC201, a TRAIL pathway-inducing compound, determines its potent anti-cancer activity. Oncotarget 2014;5:12728–37.
14. Allen JE, Krigsfeld G, Mayes PA, Patel L, Dicker DT, Patel AS, et al. Dual inactivation of Akt and ERK by TIC10 signals Foxo3a nuclear translocation, TRAIL gene induction, and potent antitumor effects. Sci Transl Med 2013;5:171ra17.
15. Bonner ER, Waszak SM, Grotzer MA, Mueller S, Nazarian J. Mechanisms of imipridones in targeting mitochondrial metabolism in cancer cells. Neuro Oncol 2021;23:542–56.
16. Ishida CT, Zhang Y, Bianchetti E, Shu C, Nguyen TTT, Kleiner G, et al. Metabolic reprogramming by dual AKT/ERK inhibition through imipridones elicits unique vulnerabilities in glioblastoma. Clin Cancer Res 2018;24:5392–406.
17. Ishizawa J, Zarabi SF, Davis RE, Halgas O, Nii T, Jitkova Y, et al. Mitochondrial ClpP-mediated proteolysis induces selective cancer cell lethality. Cancer Cell 2019;35:721–37.
18. Graves PR, Aponte-Collazo LJ, Fennell EMJ, Graves AC, Hale AE, Dicheva N, et al. Mitochondrial protease ClpP is a target for the anticancer compounds ONC201 and related analogues. ACS Chem Biol 2019;14:1020–9.
19. Prabhu VV, Morrow S, Rahman Kawakibi A, Zhou L, Ralff M, Ray J, et al. ONC201 and imipridones: Anti-cancer compounds with clinical efficacy. Neoplasia 2020;22:725–44.
20. Vasan K, Werner M, Chandel NS. Mitochondrial metabolism as a target for cancer therapy. Cell Metab 2020;32:341–52.
21. Philip PA, Buyse ME, Alistar AT, Rocha Lima CM, Luther S, Pardee TS, et al. A phase III open-label trial to evaluate efficacy and safety of CPI-613 plus modified FOLFIRINOX (mFFX) versus FOLFIRINOX (FFX) in patients with metastatic adenocarcinoma of the pancreas. Future Oncol 2019;15:3189–96.
22. Pardee TS, Anderson RG, Pladna KM, Isom S, Ghiraldeli LP, Miller LD, et al. A phase I study of CPI-613 in combination with high-dose cytarabine and mitoxantrone for relapsed or refractory acute myeloid leukemia. Clin Cancer Res 2018;24:2060–73.
23. Alistar A, Morris BB, Desnoyer R, Klepin HD, Hosseinzadeh K, Clark C, et al. Safety and tolerability of the first-in-class agent CPI-613 in combination with modified FOLFIRINOX in patients with metastatic pancreatic cancer: a single-centre, open-label, dose-escalation, phase 1 trial. Lancet Oncol 2017;18:770–8.
24. Iwamoto FM, Lamborn KR, Kuhn JG, Wen PY, Yung WK, Gilbert MR, et al. A phase I/II trial of the histone deacetylase inhibitor romidepsin for adults with recurrent malignant glioma: North American brain tumor consortium study 03-03. Neuro Oncol 2011;13:509–16.
25. Grasso CS, Tang Y, Truffaux N, Berlow NE, Liu L, Debily MA, et al. Functionally defined therapeutic targets in diffuse intrinsic pontine glioma. Nat Med 2015;21:827.
26. Masui K, Harachi M, Cavenee WK, Mischel PS, Shibata N. mTOR complex 2 is an integrator of cancer metabolism and epigenetics. Cancer Lett 2020;478:1–7.
27. Bi J, Chowdhry S, Wu S, Zhang W, Masui K, Mischel PS. Altered cellular metabolism in gliomas - an emerging landscape of actionable co-dependency targets. Nat Rev Cancer 2020;20:57–70.
28. Gimple RC, Kidwell RL, Kim LJY, Sun T, Gromovsky AD, Wu Q, et al. Glioma stem cell-specific superenhancer promotes polyunsaturated fatty-acid synthesis to support EGFR signaling. Cancer Discov 2019;9:1248–67.
29. Chowdhry S, Zanca C, Rajkumar U, Koga T, Diao Y, Raviram R, et al. NAD metabolic dependency in cancer is shaped by gene amplification and enhancer remodelling. Nature 2019;569:570–5.
30. Randall EC, Lopez BGC, Peng S, Regan MS, Abdelmoula WM, Basu SS, et al. Localized metabolomic gradients in patient-derived xenograft models of glioblastoma. Cancer Res 2020;80:1258–67.
31. Zhang G, Frederick DT, Wu L, Wei Z, Krepler C, Srinivasan S, et al. Targeting mitochondrial biogenesis to overcome drug resistance to MAPK inhibitors. J Clin Invest 2016;126:1834–56.
32. Shukla SK, Purohit V, Mehla K, Gunda V, Chaika NV, Vernucci E, et al. MUC1 and HIF-1alpha signaling crosstalk induces anabolic glucose metabolism to impart gemcitabine resistance to pancreatic cancer. Cancer Cell 2017;32:71–87.
33. Prabhu VV, Talekar MK, Lulla AR, Kline CLB, Zhou L, Hall J, et al. Single agent and synergistic combinatorial efficacy of first-in-class small molecule imipridone ONC201 in hematological malignancies. Cell Cycle 2018;17:468–78.
34. Ralff MD, Kline CLB, Kucukkase OC, Wagner J, Lim B, Dicker DT, et al. ONC201 demonstrates antitumor effects in both triple-negative and non-triple-negative breast cancers through TRAIL-dependent and TRAIL-independent mechanisms. Mol Cancer Ther 2017;16:1290–8.
35. Kline CLB, Ralff MD, Lulla AR, Wagner JM, Abbosh PH, Dicker DT, et al. Role of dopamine receptors in the anticancer activity of ONC201. Neoplasia 2018;20:80–91.
36. Pruss M, Dwucet A, Tanriover M, Hlavac M, Kast RE, Debatin KM, et al. Dual metabolic reprogramming by ONC201/TIC10 and 2-Deoxyglucose induces energy depletion and synergistic anti-cancer activity in glioblastoma. Br J Cancer 2020;122:1146–57.